Nat. Hazards Earth Syst. Sci. Discuss., 2, 7651–7678, 2014
www.nat-hazards-earth-syst-sci-discuss.net/2/7651/2014/
doi:10.5194/nhessd-2-7651-2014


Natural Hazards and Earth System Sciences
Open Access
Discussions



# Amalgamation in landslide maps: effects and automatic detection

**O. Marc and N. Hovius**

Helmholtz Centre Potsdam, German Research Center for Geosciences (GFZ), Telegrafenberg, 14473 Potsdam, Germany

Received: 27 November 2014 – Accepted: 29 November 2014 – Published: 16 December 2014

Correspondence to: O. Marc (omarc@gfz-potsdam.de)

Published by Copernicus Publications on behalf of the European Geosciences Union.







## Abstract

Inventories of individually delineated landslides are a key to understanding landslide physics and mitigating their impact. They permit assessment of area-frequency distributions and landslide volumes, and testing of statistical correlations between landslides and physical parameters such as topographic gradient or seismic strong motion. Amalgamation, i.e. the mapping of several adjacent landslides as a single polygon, can lead to potentially severe distortion of the statistics of these inventories. This problem can be especially severe in datasets produced by automated mapping. We present 5 inventories of earthquake-induced landslides mapped with different materials and techniques and affected by varying degrees of amalgamation. Errors on the total landslide volume and power-law exponent of the area-frequency distribution, resulting from amalgamation, may be up to 200 and 50 %, respectively. We present an algorithm based on image and DEM analysis, for automatic identification of amalgamated polygons. On a set of about 2000 polygons larger than 1000 $m^2$, tracing landslides triggered by the 1994 Northridge earthquake, the algorithm performs well, with only 2.7–3.6 % wrongly amalgamated landslides missed and 3.9–4.8 % correct polygons wrongly identified as amalgams. This algorithm can be used broadly to check landslide inventories and allow faster correction by automating the identification of amalgamation.

## 1 Introduction

Regional landslide maps are a crucial component of many landslide related studies (Guzzetti et al., 2012): they are necessary to improve our understanding of landslide rupture mechanics and test conceptual models, to produce landslide risk and vulnerability maps, to understand how different climatic and tectonic mechanisms can trigger landslides, and to estimate how mass wasting contributes to sediment production and landscape evolution (Montgomery and Dietrich, 1994; Meunier et al., 2007, 2008; Hovius et al., 1997). Such maps used to be created by manual mapping from





NHESSD
2, 7651–7678, 2014



remote sensed imagery, often accompanied by partial field checks (e.g. Harp et al., 1981; Harp and Jibson, 1996). Due to the high cost and time associated with manual mapping of thousands or tens of thousands of landslides over large areas, automated mapping techniques are increasingly used (e.g. Martha et al., 2010; Mondini et al., 2011; Parker et al., 2011). These techniques have specific associated errors, amongst which amalgamation, that is the bundling of several adjacent landslides into a single map polygon, is prominent. Amalgamation typically occurs when the spatial density of landslides is high and the resolution of images from which they are mapped relatively low, making it difficult to differentiate multiple landslides in a perturbed area. Automatic mapping algorithms designed to detect change of surface properties, irrespective of the shape of the changed area are especially prone to this effect. If uncorrected, amalgamation can lead to severely mistaken results and interpretations in many domains. For example, studies using landslide maps to estimate the volume of debris produced, whether to understand sediment transfer dynamics (Hovius et al., 2000; Yanites et al., 2010), organic matter mobilisation (Hilton et al., 2011), average erosion rates (Hovius et al., 1997) or mountain building (Parker et al., 2011), rely on empirical laws giving landslide volume as a function of landslide area (Guzzetti et al., 2009; Larsen et al., 2010). In this approach, landslide depth is assumed to scale with area, giving rise to strongly non-linear area–volume relations, which assign disproportionate importance to landslides with the largest surface areas. Accurate landslide area mapping, differentiating precisely between individual events is therefore of the essence (Li et al., 2014). This also applies to studies considering the area-frequency distribution of landslides, whether to assess landslide hazard and risk associated with extreme events (Malamud et al., 2004a), or to understand the underlying physics of the distribution (Pelletier et al., 1997; Stark and Guzzetti, 2009; Frattini and Crosta, 2013). Finally, any attempt to understand the physics of landslide triggering from mapped landslide patterns could suffer from the effects of wrongly mapped landslide outlines and artificial prominence of large disturbed areas (Montgomery and Dietrich, 1994; Meunier et al., 2008).





NHESSD
2, 7651–7678, 2014



Here, we survey why and where amalgamation can occur, and determine the minimum error it has introduced to estimates of total landslide volume and the area-frequency distribution of several landslide inventories. Subsequently, we propose an algorithm able to automatically detect amalgamation when provided with a raster file of polygon shapes and a DEM. Performance of this algorithm is tested on a representative subset of the inventory of landslides triggered by the Northridge earthquake. We finish with a short discussion of the benefits and limitations of this approach and possible alternatives.

## 2 Landslide mapping and amalgamation

Most landslide inventories are derived from analysis of optical or multispectral imagery, exploiting the typical texture, colour and spectral properties of freshly disturbed areas (Guzzetti et al., 2012). Often, landslides are conspicuous because they clear vegetation that has a very different appearance or radiation intensity spectrum. When landslides are mapped as polygons, whether by men or machine, the general assumption is that the polygon represents a single landslide, most often combining a scar area, a deposit area and sometimes a runout area. A mapped polygon is therefore assumed to contain direct or indirect information on the location and size and, implicitly, the volume of one landslide but also potentially about the slope where the landslide initiated and terminated, the runout distance, the drop of potential energy, or the triggering mechanism, such as the local peak ground acceleration or pore pressure at the time of failure.

Amalgamation, the combination of several individual landslides in a single polygon, can be due to the actual coalescence of landslides, or the apparent contiguity of disturbed areas in images with low resolution or poor contrast between affected and unaffected areas (Fig. 1). Indeed, where landsliding is very dense, several adjacent landslides may have joint runout areas or overlapping deposits, or scars separated by a distance too short to be resolved by the available imagery. At a given resolution, multispectral images contain more information than optical images, which may help





NHESSD
2, 7651–7678, 2014



in delineating individual landslides but this does not always preclude amalgamation in landslide mapping. Even where image resolution would permit accurate mapping of individual landslides, amalgamation can occur when the primary goal of the mapper is not to map landslide extent precisely, but rather to rapidly evaluate the area affected by slope failure. This seems to be especially common for maps predating widespread use of landslide area–volume relationships. In automatic mapping, algorithms that are not object oriented will usually classify single pixels based on their various bulk properties (Guzzetti et al., 2012). If adjacent pixels are classified as disturbed, then the algorithm will combine them in a single polygon, regardless of how many separate landslides are contained within. When image resolution is not very high, then automatic algorithms can bundle hundreds of small landslides, located within a limited area with high propensity to failure, into a single, apparently very large landslide polygon.

A striking example of amalgamation due to automated mapping procedures can be found in the JouJou Mountain area of Taiwan, where pervasive shallow landsliding occurred during the $M_w = 7.6$ ChiChi earthquake in 1999 (Fig. 2) (Liao and Lee, 2000). In available maps, these landslides have been merged into a few complex shaped polygons, blanketing the steep, gullied hills and covering 9.8 km$^2$. However, a separate, local survey has found more than one thousand individual, shallow failures, many of which adjoined without making larger landslides (Lee et al., 2010). Together, these landslides had a total area of 7.22 km$^2$, implying a significant area exaggeration by the automated mapping procedure.The implications of this extreme amalgamation are far reaching. For example, using common landslide area–volume relations (Guzzetti et al., 2009; Larsen et al., 2010), the total volume of the six largest, automatically mapped polygons in the area would be estimated at about 0.19 km$^3$, with the largest polygon (4.13 km$^2$) alone contributing about 0.11 km$^3$. If the total area occupied by these six polygons is arbitrarily repartitioned into 1000 landslides of roughly equal size, set by the characteristic local ridge spacing and slope lengths of 100–150 m, then a 17-fold reduction of the estimated landslide volume would result. This estimate could be refined with access to the local landslide data (Lee et al., 2010), which can be seen to have





NHESSD
2, 7651–7678, 2014



a non-uniform area-frequency distribution with hundreds of landslides with areas of 100 $m^2$ and one landslide of 0.1 $km^2$.

In this example, amalgamation of landslides is easily recognizable due to the complex shape of polygons straddling multiple topographic features, with surface areas much larger than permitted by the characteristic length scale of the topography. Formally, the merging of several landslides can result in a range of geometric or topographic inconsistencies, such as multi-branched polygons, or polygons with orientations inconsistent with local topographic slope or transgressing ridgelines or channels (Fig. 2). We consider that these features are unlikely characteristics of individual landslides, even though failure on multiple scarps, divergence in runout, runout crossing rivers and spreading on the opposing valley side or occasional overtopping of dividing ridges are known to happen.

Some polygons may also appear topographically and geometrically consistent, although they are, in fact, a combination of several adjacent landslides close to or below the resolution of available images, the combined effect of which is to alter the visual or spectral properties of a larger area. This blurring can conjugate amalgamation and an exaggeration of the area affected by landslides, but it cannot be identified without use of very high-resolution images (Fig. 2). It is, therefore, out of the scope of our study and remains a challenge and a caveat for landslide mapping.

## 3 Data

The recognition of geometric and topographic inconsistencies in landslide inventories is a key to identification of amalgamation of individual landslides and mitigation of its effects. To develop a method for detection of amalgams in large landslide datasets, and to evaluate the effects of amalgamation on scientifically interesting derivatives of these datasets, we have focused on earthquake cases. Large earthquakes can trigger many thousands of landslides in a limited area, reducing possible effects of geological heterogeneity on landslide populations and their statistics. Moreover, by focusing on land-





NHESSD
2, 7651–7678, 2014



slides with a shared trigger mechanism, we have removed possible complications due to convolution of trigger-specific effects from our analysis. Finally, Earthquake-induced landslide populations tend to span a very large range of landslide sizes, allowing robust computation of area-frequency statistics, one of the key attributes affected by amalgamation.

We have used 5 published inventories of earthquake-induced landslides, mapped over areas of $10^3$–$10^4$ km$^2$. Together, these inventories cover a range of mapping approaches from manual mapping with extensive field checking, to fast automated mapping with limited supervision and verification. The 1994 $M_w = 6.6$ Northridge earthquake in California triggered more than 10 000 landslides, which were mapped manually from airphotos, with field checks at selected sites (Harp and Jibson, 1996). The same approach was used to map more than 6000 landslides triggered by a $M_w = 7.6$ earthquake in 1976 in Guatemala (Harp et al., 1981). The 1999, $M_w = 7.6$ ChiChi earthquake in west Taiwan also caused severe landsliding, with more than 9000 landslides larger than 625 m$^2$ (25 m × 25 m) mapped automatically from SPOT satellite imagery and then manually checked by Liao and Lee (2000). Finally, for the 2008, $M_w = 7.9$ Wenchuan earthquake in China, many different maps of coseismic landslides exist (Ouimet, 2010; Qi et al., 2010; Dai et al., 2011; Gorum et al., 2011; Parker et al., 2011; Xu et al., 2014), allowing comparison of independent and broadly equivalent datasets. We have used two catalogues containing 50 000 polygons apiece. One was mapped with a semi-automatic algorithm using 2.5 to 10 m-resolution SPOT 5 and EO-1 satellite imagery (Parker et al., 2011). The other was mapped by hand, mainly from 15 m-resolution ASTER imagery and locally higher resolution imagery (Gorum et al., 2011). In all these inventories, the entire area perturbed by a landslide, including scar, runout and deposit, is delineated by a single polygon.

In addition to these five inventories, we have used Aster GDEM-30 m data to evaluate the topographic context of mapped landslide polygons and as an input of our algorithm for detection of amalgams. In the case of the Wenchuan earthquake, we have also used 15 m-resolution ASTER images and 2.5 m-resolution SPOT 5 images from the





NHESSD
2, 7651–7678, 2014



epicentral area, taken shortly after the earthquakes, to verify the different landslide maps.

## 4 Quantifying effects of amalgamation

The earthquake-induced landslide inventories summarized above are too large for comprehensive manual verification. To assess the possible effects of amalgamation in these data sets, we have focused on the largest polygons in each inventory. These polygons dominate landslide volume estimates and can strongly influence the best fits to area-frequency distributions. Thus, by checking and correcting a limited number of large polygons, the quality of derivatives of landslide inventories can be substantially improved. In checking individual polygons, we considered as anomalous any polygon displaying a geometrical or topographical inconsistency such as branching, traversing of ridges or rivers or orientation inconsistent with the local topographic slope. These polygons were compared with local topographic data and, when appropriate split to make residual polygons more consistent with the general topography. Nevertheless it is clear that without high-resolution imagery, many landslide polygons were redefined in a relatively crude way.

We have used published area–volume relationships to estimate the volume of landslides from the mapped disturbed areas (Larsen et al., 2010). It was assumed that landslides with area $> 100\,000\,\mathrm{m}^2$ involved bedrock, and that smaller landslides were mixed bedrock and soil failures. Landslide maps typically do not distinguish between scar and deposit, lumping the two in one area measure. According to Larsen et al. (2010), scars and deposits have area–volume relations with the same power-law exponent, implying constant size ratios between scar and deposit areas of 1.1 and 1.9 for mixed and bedrock landslides, respectively. Hence, we have estimated the scar area by dividing the mapped landslide area by 2.1 and 2.9 for mixed and bedrock landslides, respectively, assuming that runout was equal to the scar length. Then we converted scar area $A$, into volume $V$, for bedrock and soil landslides with $V = aA^b$ with $a = 0.146$ and





NHESSD
2, 7651–7678, 2014



0.234 and $b$ = 1.33 and 1.41 for mixed and bedrock landslides, respectively. Computed landslide individual and total volumes appear to be consistent with field estimates for cases where the whole perturbed area is mapped.

Comprehensive landslide inventories have a typical area-frequency distribution with a roll-over and a power-law decay with an exponent, $\rho$, commonly within a narrow range of values (Malamud et al., 2004b). The roll-over can be caused by censoring of the small landslides due to the mapping resolution (Stark and Hovius, 2001), but can also be related to the physics of landsliding and the transition from cohesion-controlled to friction-controlled hillslope stability with increasing landslide area and depth (Katz and Aharonov, 2006; Stark and Guzzetti, 2009). The roll-over and power-law decay have also been attributed to a combination of the size distribution of continuous local topographic slopes and the distribution of moisture or increasing cohesion with depth (Pelletier et al., 1997; Frattini and Crosta, 2013). We have assessed the impact of amalgamation by comparing the area-frequency distribution of the original datasets with that of our partially corrected datasets. Because the frequency decay with increasing landslide size is usually modeled as a power-law, a specific functional form does not have to be prescribed if we only consider the distribution at areas ten times larger than the roll-over. For these large areas we have obtained $\rho$ with a linear least-square regression of the log-transformed data (Fig. 3).

In many cases a larger number of smaller polygons were also visibly amalgamated, but we did not correct them, due to the effort and uncertainties involved. Thus, the estimates of errors on total landslide volume and the power law exponent of the landslide area-frequency distribution due to amalagamation, presented below, are likely minimum values. Next, we review the individual landslide inventories and highlight the varying degrees to which they are affected by amalgamation and its effects.

Landslides induced by the 1976 Guatemala and 1994 Northridge earthquakes were mapped in detail, apparently to record where landslides had occurred, but not necessarily to distinguish the boundaries of individual landslides. We have inspected all 356 polygons with an area larger 10 000 $m^2$ in the Northridge inventory and all 90 polygons





NHESSD
2, 7651–7678, 2014



exceeding 100 000 $m^2$ in the Guatemala dataset. Together, these polygons represent 56 and 73 % of the uncorrected volume of the landslide populations of the Northridge and Guatemala earthquakes, respectively. 162, respectively 51 of these polygons were found to be amalgams of several landslides. They were split according to their shapes and relation to the local topography. This resulted in a reduction of the total volume of landslides by 16 % in the Northridge case and 35 % in the Guatemala case, and an increase of the area-frequency scaling exponent, by 16 and 22 %, from 1.57 and 1.33 to 1.82 and 1.62, respectively (Fig. 3).

The ChiChi earthquake caused widespread landsliding in the mountains of central west Taiwan. An inventory of these landslides (Liao and Lee, 2000) contains 9272 polygons in an area 150 times larger than the JouJou Mountain, mentioned above, with a total estimated volume of about 0.73 $km^3$. We have inspected all 173 polygons larger 100 000 $m^2$, representing 85 % of the total uncorrected volume of the ChiChi inventory. We have found that 100 of them needed corrections ranging from the splitting of minor branches to the artificial fragmentation of the largest polygons in the JouJou mountain area, where precise correction was impossible. Together, these corrections resulted in a volume reduction of 38 % to 0.45 $km^3$, but an insignificant increase of the area-frequency scaling exponent by 5 %.

The two inventories for the Wenchuan earthquake have similar total landslide areas and similar total numbers of landslides, even though the mapping of Gorum et al. (2011) extended further to the North along the seismogenic fault. We have compared the maps where they overlap, along 150 km of the fault trace, where the majority of landslides occurred (e.g. Fig. 2). There is good overall agreement between the data sets, but the manual mapping of Gorum et al. (2011) has clearly delineated many more individual slides (Fig. 2). Many examples of amalgamation are evident in the Parker et al. (2011) data set (Fig. 1), and although, there are some mapping discrepancies between the two inventories, this appears to be the main difference between them. It has resulted in a total landslide volume reduction of 69 %, from 6.30 $km^3$ for the automated-mapping inventory (Parker et al., 2011) to 1.96 $km^3$ for the original manually-mapped





NHESSD
2, 7651–7678, 2014



inventory of Gorum et al. (2011). However, this inventory also contains amalgamation artefacts (Fig. 2). We have visually checked all 152 landslides larger than 300 000 $m^2$, representing 51 % of the total volume of the manual inventory (including landslides mapped in areas not surveyed by Parker et al., 2011). Of these 87 required editing, leading to a final landslide volume estimate of 2.3 $km^3$ instead of 2.45 $km^3$, equivalent to a modest reduction of 6 %.

The landslide polygon area-frequency distributions of the Wenchuan inventories also differ significantly (Fig. 3). First, the amalgamated catalogue of Parker et al. (2011) yields a discontinuous distribution, which does not exhibit the roll-over commonly observed in well-mapped data sets (Malamud et al., 2004b; Brardinoni and Church, 2004). Instead the smaller polygons also have a decreasing frequency with increasing size, and they appear to be relatively infrequent compared to medium to large slides. In contrast, the manually mapped inventory has a area-frequency distribution with a rollover at 1000 $m^2$. The exponent on the best-fit power-law for this data set, after our correction for amalgamation is also much higher than for the Parker et al. (2011) inventory, $\rho = 1.5$ and $\rho = 1.0$, respectively, confirming the relative abundance of large, mostly amalgamated polygons in the latter (Figs. 1 and 2). Correction for amalgamation effects results in a slight rise of the scaling exponent of the manually mapped inventory to $\rho = 1.6$.

From these analyses it is clear that amalgamation can significantly distort both landslide population volume estimates and the frequency distribution of mapped landslide areas. However, the frequency distribution itself does not necessarily betray amalgamation, and exhaustive visual screening can be prohibitively time consuming. In the following section, we propose an automatic algorithm, which can be used to differentiate correctly mapped and amalgamated polygons and allow faster and more comprehensive cleaning of affected data sets.





NHESSD
2, 7651–7678, 2014



## 5 Automatic detection of amalgamation

Because amalgamation leads to geometric anomalies and unusual positions of putative landslides in the landscape it is possible to detect amalgams simply by looking at their shape and at the underlying topography. Following the criteria defined in Sect. 2 (Landslide mapping and amalgamation) we have developed an algorithm able to guide a mapper or an end-user towards suspicious polygons, and facilitate a correction or an assessment of the catalogue quality. The algorithm requires a DEM, a raster made from the polygon shapefile and a text file with polygon ID and information. Below, we present the operation of the algorithm and assess its accuracy.

First, the algorithm considers the geometry of a landslide polygon. The branching of polygons is the most common and visible effect of amalgamation. This affects the relation between perimeter, $P$, and area $A$, of the polygons, biasing amalgams towards high $P$. These attributes are easily extracted from a landslide inventory with any GIS. A polygon with given $P$ and $A$ can be compared to an ellipse of equal $P$ and $A$, and aspect ratio $K$. Using Fagnano (1750) approximation, ellipse perimeter can be written as:

$$P = \pi\left(\frac{3}{2b}(K+1) - \sqrt{Kb^2}\right) \tag{1}$$

where $b$ is the smallest radius. Since $A = \pi K b^2$, it can be shown that the perimeter of any ellipse varies as

$$P = \left(\frac{3(K+1)}{2\sqrt{K}} - 1\right)\sqrt{\pi A}. \tag{2}$$

Rearranging Eq. (2), $K$ can be found from $P$ and $A$ as the solution of a second order equation:

$$K = \frac{1}{2}\left(\frac{4}{9}\left(\frac{P}{\sqrt{\pi A}}+1\right)^2 - 2 + \sqrt{\left(\frac{4}{9}\left(\frac{P}{\sqrt{\pi A}}+1\right)^2 - 2\right)^2 - 4}\right). \tag{3}$$





NHESSD
2, 7651–7678, 2014



Thus, any polygon can be described easily and objectively by the aspect ratio, $K$, of its equivalent ellipse. For reference, a circle would yield $K = 1$, a square $K = 2.3$ and rectangle twice as long as wide $K = 2.7$. A polygon with high $K$ is more likely to be incorrect whereas a polygon with $K < 2$ has a compact shape from which any mapping error can not easily be recognized. Therefore, to accelerate the algorithm any polygon below a critical aspect ratio, $K_c$, is assumed to be correct (Fig. 4).

A high $K$ value may signal amalgamation or simply an elongated landslide, for example due to long runout. Therefore, $K$ is a useful input parameter but ultimately it is necessary to explicitly consider the geometry of the polygon. This is achieved by reducing the mapped polygons to their skeleton with a standard image analysis method, which iteratively thins a solid polygon to a branched centre-line (Fig. 5). From this skeleton, branch points and individual branches are easily found. However, even polygons with a relatively simple shape may have skeletons with some branching points and small branches pointing towards a polygon corner or irregular side. To eliminate these spurious branches, we impose an arbitrary threshold size ratio of branches relative to the longest branch, $RB_c$. A polygon with a main branch and several smaller branches, all of which are shorter than the main branch by a factor $1/RB_c$ or more is considered to be a correctly mapped, single landslide (Fig. 4). All other polygons receive a score equal to the number of branches, longer than the longest branch divided by $RB_c$, reflecting qualitatively the degree of amalgamation.

In a second step, the algorithm tests the consistency of a polygon with apparently correct geometry, with the local topography. This is done by extracting the DEM elevation along the longest branch of the polygon, which is assumed to be an adequate representation of the pathway of the landslide. First, the algorithm checks that all elevations along the branch are within the elevation range bracketed by the branch endpoints. A violation of this condition typically signals that the branch traverses a ridge or valley floor, or that two landslides were merged into a crescent shaped polygon, smooth enough not to be identified as a likely amalgam by the first part of the algorithm. If the polygon passes this second test, then a last check is made to see if the





NHESSD
2, 7651–7678, 2014



maximum variation of elevation along the main branch is above the minimum slope for landsliding, $S_c$ (Fig. 4). Polygons failing this test are typically oriented perpendicular to the main topographic slope over long distances, as a result of the lateral merging of several small, parallel failures along a ridge or cliff.

Thus, our algorithm is formally based on 3 adjustable parameters $K_c$, $RB_c$, and $S_c$. Of these, only $RB_c$ may be substantially tuned, depending on the smoothness of the input raster, which in turn depends on the landslide mapping technique and the raster resolution.

$S_c$ is a physical parameter which should normally be close to a 10° threshold for landsliding (e.g. Meunier et al., 2007; Lin et al., 2008), thus requiring minimal tuning, unless the local substrate has exceptional properties. To minimize the number of false negatives (i.e. undetected amalgams), $K_c$ should be set at a low value of about 2, so that only polygons without any geometrical complexity are screened out. Setting $K_c$ at a higher value can be useful to assess the degree of amalgamation and isolate only those polygons that are likely to be composites of many landslides.

To assess the accuracy of the algorithm we have applied it to an inventory of landslides triggered by the 1994 Northridge earthquake in southern California (Harp and Jibson, 1996). Within the bounds of the Santa Susanna Mountains, we manually screened all 2083 mapped polygons larger than 1000 $m^2$ for amalgamation. This is close to the rollover in the landslide area-frequency distribution of the inventory, so that the test set encompasses most of the landslide volume. The Santa Susanna subset is representative of the diversity of size and shape that can be found in the Northridge inventory in its entirety. Of all polygons in the subset, the amalgamation state of 136 (6.52 %) could not be ascertained visually. These polygons were removed from the test data set before further analysis. Of the remaining 1950 polygons, 617 amalgams and 1187 single landslides were correctly classified by our algorithm. The algorithm missed 70 amalgams (3.6 % of false negatives) and wrongly classified 76 single landslides as amalgams (3.9 % of false positives) (Table 1). About two thirds of all polygons classified as amalgams were detected using the branching criterium, in part because it is





NHESSD
2, 7651–7678, 2014



the most easily detectable feature but also because it is the first step of the algorithm. One third of amalgamation cases were only diagnosed by the second step of the algorithm, which considers the topographic context of a polygon. Taking results from these two steps together, the overall accuracy of the algorithm was very good, with 1804 of 1950 (92.5 %) polygons in the test set classified correctly (Table 1). Thus, our algorithm provides a relatively rapid and accurate way to assess the quality of a dataset and a partial guide to manual correction. It can reduce the workload associated with manual splitting of amalgamated polygons, by foreshortening the amalgam identification phase, and enhancing the detection of smaller amalgamated polygons that may have only subtle distortions. However, the algorithm only yields a minimal number of branches and the automatic and accurate splitting of complex polygons based on detected branching geometry remains a challenge.

The algorithm can assess the quality of every polygon of an inventory as long as the raster resolution is high enough for a polygon to be made up by at least a few tens of pixels, so that a skeleton can be defined. Therefore, at a raster pixel size of 2 m, 100 $m^2$ polygons would have about 25 pixels and could be analysed by our algorithm. This is lower than the usual roll-over of landslide area-frequency distribution (e.g. Malamud et al., 2004b; Brardinoni and Church, 2004). DEMs with a high spatial resolution will also yield better results and the accuracy of the detection is helped by the fact that the algorithm uses raw elevation data rather than a local derivative such as slope, which is calculated over several adjacent pixels.

## 6 Discussion

We have proposed an algorithm based on polygon geometry and topographic analysis, which allows automatic detection of polygons outlining amalgamated landslides with good but incomplete detection rates and minimal diagnostic error. However, depending on the objective of a study, even a few wrongly diagnosed polygons may be of concern. Therefore, the algorithm must be tuned towards a reduction of false negative results,





NHESSD
2, 7651–7678, 2014



by increasing $RB_c$ or $S_c$, even if the rate of false positive results increases as a consequence. For example, raising $RB_c$ from 5 to 6 in the analysis of landslides in the Santa Susanna Mountains results in a useful 24 % reduction of false negative results, from 70 to 52 polygons out of 1950, and a concomitant increase of false positive results by 16 % from 76 to 90 polygons (Table 1). This increase of false positives is not an issue, if amalgams detected by the algorithm are subsequently split manually. In that case, the operator can decide to leave an incorrectly diagnosed polygon intact. However, false negatives will go unnoticed and could have a large impact. Therefore, it is advisable to perform an additional manual check of the largest polygons in a data set, irrespective of how the classification algorithm has diagnosed them, especially for applications where the importance of polygons is proportional to their size. For example, one false negative within the 10 or 20 largest landslides in an inventory could significantly affect estimated total landslide volume.

A second, more fundamental issue is that the algorithm considers polygon geometry, in a way which does not allow detection of ellipsoid-shaped amalgams. Examples of this can be found, amongst others, in an inventory of landslides triggered by the 2008 Wenchuan earthquake (Gorum et al., 2011), where several landslides on the same slope were sometimes merged into larger, relatively smooth, polygons with a low $K$ value and without any clear geometric or topographic indication of amalgamation (Fig. 2). In this case, image resolution may have been too low to distinguish the separate landslides, or the mapper may have simplified the geometry for convenience. For such amalgams, even if another criteria, such as alignment of the polygon long axis with the strike of the topographic slope, hints at possible amalgamation, high-resolution imagery would be required to test the diagnosis, as single landslides with similar shape and orientation may exist. Merger of parallel landslide outlines due to image resolution limitations may cause errors of similar magnitude as other types of amalgamation, which are more easily detected, and could critically affect the common argument that at a given pixel resolution small landslides are missed but everything above a cutoff lengthscale of a few pixels is properly mapped. Because the high-resolution imagery





NHESSD
2, 7651–7678, 2014



required to check visually for the occurrence of low-$K$ amalgamation, or any other type of amalgamation, is rarely available to end-users of landslide inventories, it is important that it is mitigated for by those who develop the mapping techniques and acquire the landslide inventories. This may not always concur with the principal objectives of a particular mapping effort, for example in natural disasters when rapid assessment of the location and total extent of landslides is of the essence. However, if a landslide inventory is to be of general use to the research community, then the risk of amalgamation must be suppressed, both in manual and automatic mapping.

Suppression of landslide polygon amalgamation is hampered by deeper issues, such as image resolution and the uncontrolled subjectivity introduced in binary landslide mapping, where every pixel either is or is not a landslide. We draw into question the general assumption that in a given inventory, every landslide larger than a few image pixels is correctly mapped (e.g. Liao and Lee, 2000). Instead, it is reasonable to expect that many disturbed areas mapped as single medium to large landslides could in fact consist of groups of smaller landslides, giving potentially significantly different erosion volumes and size statistics (Fig. 2). Moreover, satellite imagery does not always yield unambiguous information about the number and shape of landslides, which occurred on a given slope. Where this applies, subjective choices of the mapper are crystallized within the landslide inventory. A Bayesian approach to mapping, aimed at delivering probabilistic instead of binary maps (e.g. Mondini et al., 2013) could be helpful in testing the different possibilities of splitting complex disturbed areas (see Fig. 2) and ultimately deliver more accurate, objective and reproducible datasets.

Short of a practicable, comprehensive solution, our method, which has a good reliability, can be used in several ways to mitigate for amalgamation in landslide maps, by helping the mapper to identify mistakes in automatic mapping, and the user to do the same in existing landslide maps. Notably, sorting mapped polygons by $K$ value and size allows rapid, first order vetting of the largest landslides, which, when followed by manual splitting of amalgams, will be enough to yield a reasonable estimate of the total volume of landslides in an inventory. Then, for large populations, one could exclude all





NHESSD
2, 7651–7678, 2014



polygons with $K$ values above a threshold and consider the correlation between the size or location of remaining landslides and physical parameters such as local topographic slope or triggering effects. Finally, a $K$ value criteria might also be introduced in a semi automatic algorithm detecting landslides, to guide iteratively towards a sound splitting of adjoining landslides.

## 7 Conclusions

We have shown that amalgamation, the bundling of several adjacent landslides into a single map polygon is a common problem in landslide inventories that has inflated estimates of landslide volumes by up to a factor of three, and the power-law exponent of landslide area-frequency distributions by up to 50 %. Even though the design of comprehensive and fully reliable automatic corrective method remains a challenge, we have presented and tested a practical algorithm for automatic detection of amalgamated polygons based on geometric and topographic considerations. The algorithm performs well with an accuracy of 92.5 % and only 2.7–3.6 % amalgams missed and 3.9–4.8 % correct mapped polygons wrongly classified. It can, therefore, be used to automate the identification of landslide amalgams, accelerate the evaluation of datasets, and guide the manual correction of amalgams. Thus, our algorithm is a first step towards setting a quality standard for landslide maps in order to derive scientifically and societally useful variables, such as risk estimates, erosion rates, organic matter fluxes, or correlations between landsliding and physical triggers, as accurately as possible. Further challenges lie in attempting to automatically correct amalgamation and in assessing how mapping errors due to resolution blurring propagate into final products derived from landslide maps.





NHESSD
2, 7651–7678, 2014



*Acknowledgements.* O. Marc is funded by a fellowship in the EU Marie Curie International Training Network TOPOMOD, project reference number 264517. The authors have gratefully used Aster GDEM V2, a product of METI and NASA. The authors benefited from discussions with Jens Turowski and Patrick Meunier on an earlier version of the manuscript and are grateful to Tolga Gorum and Robert Parker for providing access to their landslide maps.

O. Marc and N. Hovius conceived the study and wrote the manuscript. O. Marc performed all analyses and developed the algorithm, assisted by N. Hovius. The authors have no conflicts of interest related to the work reported in this paper.

The service charges for this open access publication have been covered by a Research Centre of the Helmholtz Association.

## References

Brardinoni, F. and Church, M.: Representing the landslide magnitude–frequency relation: Capilano River basin, British Columbia, Earth Surf. Proc. Land., 29, 115–124, doi:10.1002/esp.1029, 2004. 7661, 7665

Dai, F. C., Xu, C., Yao, X., Xu, L., Tu, X. B., and Gong, Q. M.: Spatial distribution of landslides triggered by the 2008 Ms 8.0 Wenchuan earthquake, China, J. Asian Earth Sci., 40, 883–895, doi:10.1016/j.jseaes.2010.04.010, 2011. 7657

Fagnano, G.: Produzioni matematiche del conte Giulio Carlo di Fagnano, Gavelliana, 1750. 7662

Frattini, P. and Crosta, G. B.: The role of material properties and landscape morphology on landslide size distributions, Earth Planet. Sc. Lett., 361, 310–319, doi:10.1016/j.epsl.2012.10.029, 2013. 7653, 7659

Gorum, T., Fan, X., van Westen, C. J., Huang, R. Q., Xu, Q., Tang, C., and Wang, G.: Distribution pattern of earthquake-induced landslides triggered by the 12 May 2008 Wenchuan earthquake, Geomorphology, 133, 152–167, 2011. 7657, 7660, 7661, 7666, 7675, 7676

Guzzetti, F., Ardizzone, F., Cardinali, M., Rossi, M., and Valigi, D.: Landslide volumes and landslide mobilization rates in Umbria, central Italy, Earth Planet. Sc. Lett., 279, 222–229, 2009. 7653, 7655





NHESSD

2, 7651–7678, 2014



Guzzetti, F., Mondini, A. C., Cardinali, M., Fiorucci, F., Santangelo, M., and Chang, K.-T.: Landslide inventory maps: new tools for an old problem, Earth-Sci. Rev., 112, 42–66, doi:10.1016/j.earscirev.2012.02.001, 2012. 7652, 7654, 7655

Harp, E. L. and Jibson, R.: Landslides triggered by the 1994 Northridge, California, earthquake, B. Seismol. Soc. Am., 86, 319–332, 1996. 7653, 7657, 7664

Harp, E. L., Wilson, R. C., and Wieczorek, G. F.: Landslides from the February 4, 1976, Guatemala earthquake, USGS Prof. Pap. 1204 A, USGS, http://pubs.er.usgs.gov/publication/pp1204A (last access: December 2014), 1981. 7653, 7657

Hilton, R. G., Meunier, P., Hovius, N., Bellingham, P. J., and Galy, A.: Landslide impact on organic carbon cycling in a temperate montane forest, Earth Surf. Proc. Land., 36, 1670–1679, doi:10.1002/esp.2191, 2011. 7653

Hovius, N., Stark, C. P., and Allen, P. A.: Sediment flux from a mountain belt derived by landslide mapping, Geology, 25, 231–234, doi:10.1130/0091-7613(1997)025<0231:SFFAMB>2.3.CO;2, 1997. 7652, 7653

Hovius, N., Stark, C. P., Hao Tsu, C., and Jiun Chuan, L.: Supply and removal of sediment in a landslide dominated mountain belt: central range, Taiwan, J. Geol., 108, 73–89, doi:10.1086/jg.2000.108.issue-1, 2000. 7653

Katz, O. and Aharonov, E.: Landslides in vibrating sand box: what controls types of slope failure and frequency magnitude relations?, Earth Planet. Sc. Lett., 247, 280–294, doi:10.1016/j.epsl.2006.05.009, 2006. 7659

Larsen, I., Montgomery, D., and Korup, O.: Landslide erosion controlled by hillslope material, Nat. Geosci., 3, 247–251, 2010. 7653, 7655, 7658

Lee, S. T., Yu, T. T., Peng, W. F., and Wang, C. L.: Incorporating the effects of topographic amplification in the analysis of earthquake-induced landslide hazards using logistic regression, Nat. Hazards Earth Syst. Sci., 10, 2475–2488, doi:10.5194/nhess-10-2475-2010, 2010. 7655

Li, G., West, A. J., Densmore, A. L., Jin, Z., Parker, R. N., and Hilton, R. G.: Seismic mountain building: landslides associated with the 2008 Wenchuan earthquake in the context of a generalized model for earthquake volume balance, Geochem. Geophy. Geosy., 15, 833–844, doi:10.1002/2013GC005067, 2014. 7653

Liao, H.-W. and Lee, C.: Landslides triggered by Chi-Chi earthquake, in: Proceedings of the 21st Asian Conference on Remote Sensing, 1, Taipei, 383–388, 2000. 7655, 7657, 7660, 7667





NHESSD

2, 7651–7678, 2014



Lin, G. W., Chen, H., Hovius, N., Horng, M. J., Dadson, S., Meunier, P., and Lines, M.: Effects of earthquake and cyclone sequencing on landsliding and fluvial sediment transfer in a mountain catchment, Earth Surf. Proc. Land., 33, 1354–1373, doi:10.1002/esp.1716, 2008. 7664

Malamud, B., Turcotte, D., Guzzetti, F., and Reichenbach, P.: Landslides, earthquakes, and erosion, Earth Planet. Sc. Lett., 229, 45–59, 2004a. 7653

Malamud, B., Turcotte, D., Guzzetti, F., and Reichenbach, P.: Landslide inventories and their statistical properties, Earth Surf. Proc. Land., 29, 687–711, 2004b. 7659, 7661, 7665

Martha, T. R., Kerle, N., Jetten, V., van Westen, C. J., and Kumar, K. V.: Characterising spectral, spatial and morphometric properties of landslides for semi-automatic detection using object-oriented methods, Geomorphology, 116, 24–36, doi:10.1016/j.geomorph.2009.10.004, 2010. 7653

Meunier, P., Hovius, N., and Haines, A.: Regional patterns of earthquake-triggered landslides and their relation to ground motion, Geophys. Res. Lett., 34, L20408, doi:10.1029/2007GL031337, 2007. 7652, 7664

Meunier, P., Hovius, N., and Haines, J.: Topographic site effects and the location of earthquake induced landslides, Earth Planet. Sc. Lett., 275, 221–232, 2008. 7652, 7653

Mondini, A. C., Guzzetti, F., Reichenbach, P., Rossi, M., Cardinali, M., and Ardizzone, F.: Semi-automatic recognition and mapping of rainfall induced shallow landslides using optical satellite images, Remote Sens. Environ., 115, 1743–1757, doi:10.1016/j.rse.2011.03.006, 2011. 7653

Mondini, A. C., Marchesini, I., Rossi, M., Chang, K.-T., Pasquariello, G., and Guzzetti, F.: Bayesian framework for mapping and classifying shallow landslides exploiting remote sensing and topographic data, Geomorphology, 201, 135–147, doi:10.1016/j.geomorph.2013.06.015, 2013. 7667

Montgomery, D. R. and Dietrich, W. E.: A physically based model for the topographic control on shallow landsliding, Water Resour. Res., 30, 1153–1171, doi:10.1029/93WR02979, 1994. 7652, 7653

Ouimet, W. B.: Landslides associated with the May 12, 2008 Wenchuan earthquake: implications for the erosion and tectonic evolution of the Longmen Shan, Tectonophysics, 491, 244–252, doi:10.1016/j.tecto.2009.09.012, 2010. 7657





NHESSD
2, 7651–7678, 2014



Parker, R., Densmore, A., Rosser, N., De Michele, M., Li, Y., Huang, R., Whadcoat, S., and Petley, D.: Mass wasting triggered by the 2008 Wenchuan earthquake is greater than orogenic growth, Nat. Geosci., 4, 449–452, 2011. 7653, 7657, 7660, 7661, 7674, 7676

Pelletier, J. D., Malamud, B. D., Blodgett, T., and Turcotte, D. L.: Scale-invariance of soil moisture variability and its implications for the frequency-size distribution of landslides, Eng. Geol., 48, 255–268, doi:10.1016/S0013-7952(97)00041-0, 1997. 7653, 7659

Qi, S., Xu, Q., Lan, H., Zhang, B., and Liu, J.: Spatial distribution analysis of landslides triggered by 2008.5. 12 Wenchuan Earthquake, China, Eng. Geol., 116, 95–108, 2010. 7657

Stark, C. P. and Guzzetti, F.: Landslide rupture and the probability distribution of mobilized debris volumes, J. Geophys. Res.-Earth, 114, F00A02, doi:10.1029/2008JF001008, 2009. 7653, 7659

Stark, C. P. and Hovius, N.: The characterization of landslide size distributions, Geophys. Res. Lett., 28, 1091–1094, doi:10.1029/2000GL008527, 2001. 7659

Xu, C., Xu, X., Yao, X., and Dai, F.: Three (nearly) complete inventories of landslides triggered by the May 12, 2008 Wenchuan $M_w$ 7.9 earthquake of China and their spatial distribution statistical analysis, Landslides, 3, 441–461, doi:10.1007/s10346-013-0404-6, 2014. 7657

Yanites, B., Tucker, G., Mueller, K., and Chen, Y.: How rivers react to large earthquakes: evidence from central Taiwan, Geology, 38, 639–642, 2010. 7653





NHESSD

2, 7651–7678, 2014



**Table 1.** Confusion matrix of the algorithm tested on the 1950 independently verified polygons larger than 1000 $m^2$, from an inventory of landslides triggered by the 1994 Northridge earthquake. Positive and negative conditions refers to polygons considered amalgamated and correct, respectively. Values are given as number of landslides and percent of the total population. The algorithm was run with the following parameters: resolution 2 m, $K_c = 2$, $S_c = 12°$ and $RB_c = 5$ for the upper part of the table and $RB_c = 6$ for the lower part.

| | | |
|---|---|---|
| True positive: 617 (31.6 %) | False positive: 76 (3.9 %) | Positive predictive rate = 89.0 % |
| False negative: 70 (3.6 %) | True negative: 1187 (60.9 %) | Negative predictive rate = 94.4 % |
| Sensitivity = 89.8 % | Specificity = 94.0 % | Accuracy = 92.5 % |
| True positive: 653 (33.5 %) | False positive: 94 (4.8 %) | Positive predictive rate = 87.4 % |
| False negative: 52 (2.7 %) | True negative: 1151 (59.0 %) | Negative predictive rate = 95.7 % |
| Sensitivity = 92.6 % | Specificity = 92.5 % | Accuracy = 92.5 % |





NHESSD
2, 7651–7678, 2014



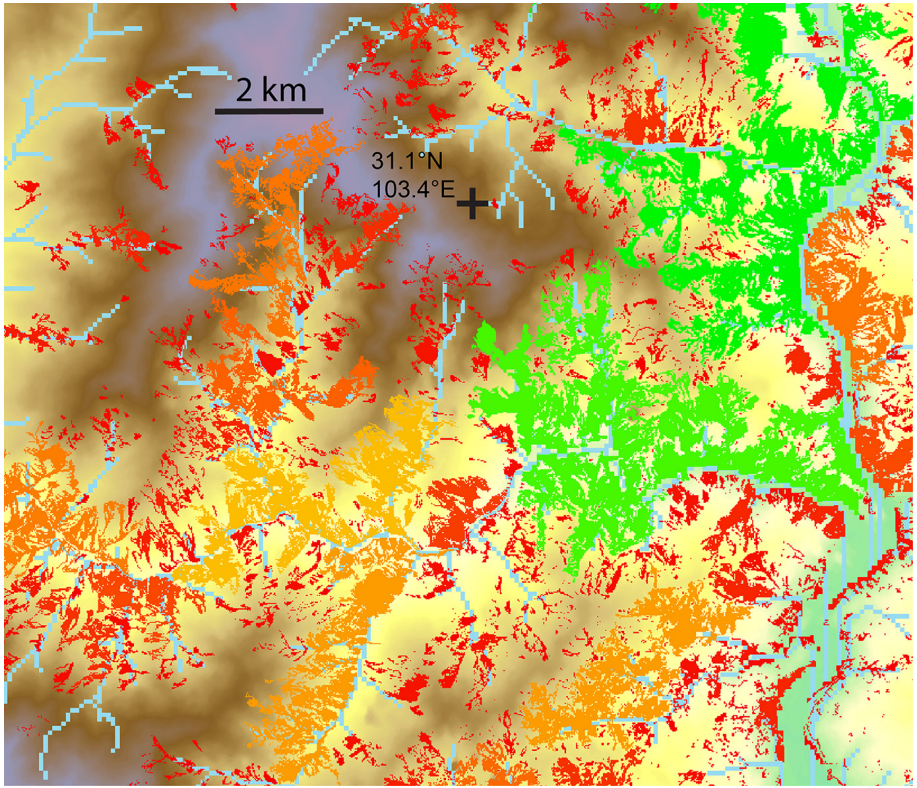


**Figure 1.** Some polygons from the Parker et al. (2011) dataset, representing landsliding caused by the 2008 Wenchuan earthquake. Polygons are color coded by size (red being the smaller polygons) and overlaid on a DEM and a river network. The density of landsliding is correctly estimated but dozens of small landslides have been connected along slope or even across rivers or ridges. Light orange and green polygons have total area larger than 1 $km^2$.





NHESSD
2, 7651–7678, 2014

Amalgamation in landslide maps: effects and automatic detection

O. Marc and N. Hovius



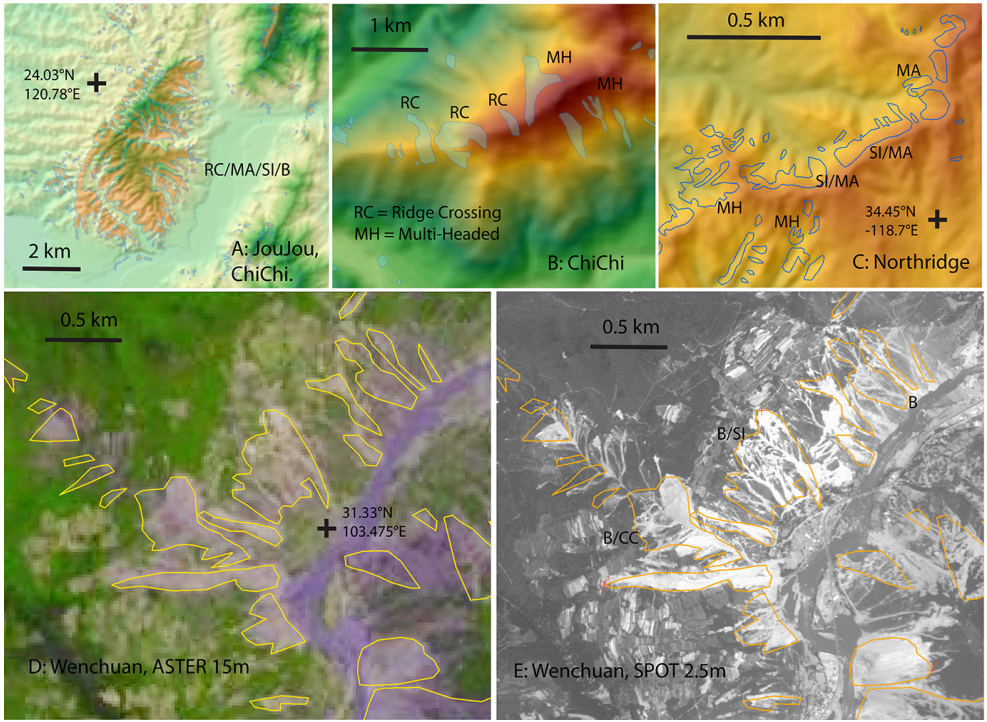


**Figure 2. (a)–(c)** Landslide polygons on a DEM topography showing examples of amalgamation in the ChiChi and Northridge inventories. Geometric and topographic inconsistencies that signal amalgamation are specified as follow: RC for ridge crossing, CC for channel crossing, MH for multi-headed, MA for multi-armed and SI for slope inconsistencies. **(d, e)** Some polygons mapped by Gorum et al. (2011) after the Wenchuan earthquake overlaid on a 15 m-resolution ASTER image **(d)** and on a 2.5 m-resolution SPOT 5 image **(e)**, of the same area. Note the presence of amalgamation but also the significant mapping extent exaggeration when mapping on low resolution relative to the landslide density.





NHESSD
2, 7651–7678, 2014



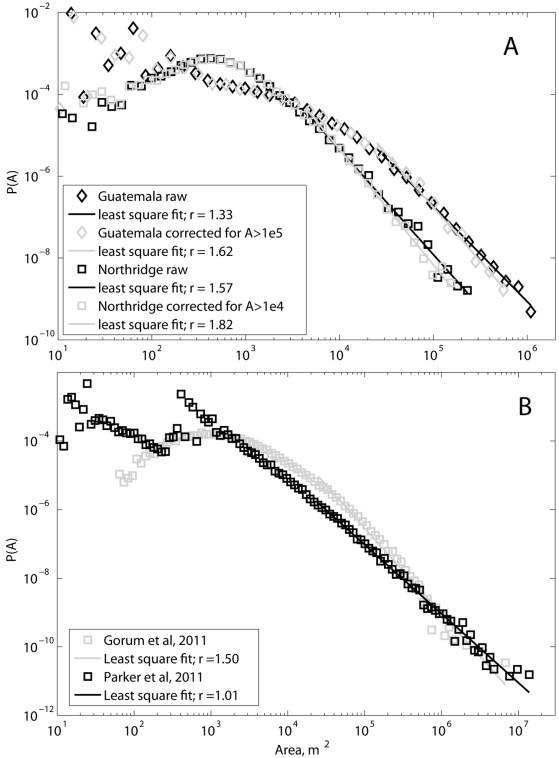


**Figure 3.** Amalgamation effect on landslide area-frequency distributions. **(a)** Comparison between the raw data from the coseismic landslide maps for to the 1976 Guatemala and 1994 Northridge earthquakes and the corrected catalogue where every amalgam larger than 100 000 $m^2$ and 10 000 $m^2$ was split, respectively. **(b)** For the 2008 Wenchuan earthquake, several landslide maps were published. Of these, the Parker et al. (2011) dataset is severely affected by amalgamation whereas the Gorum et al. (2011) dataset is relatively exempt from amalgams.





NHESSD
2, 7651–7678, 2014



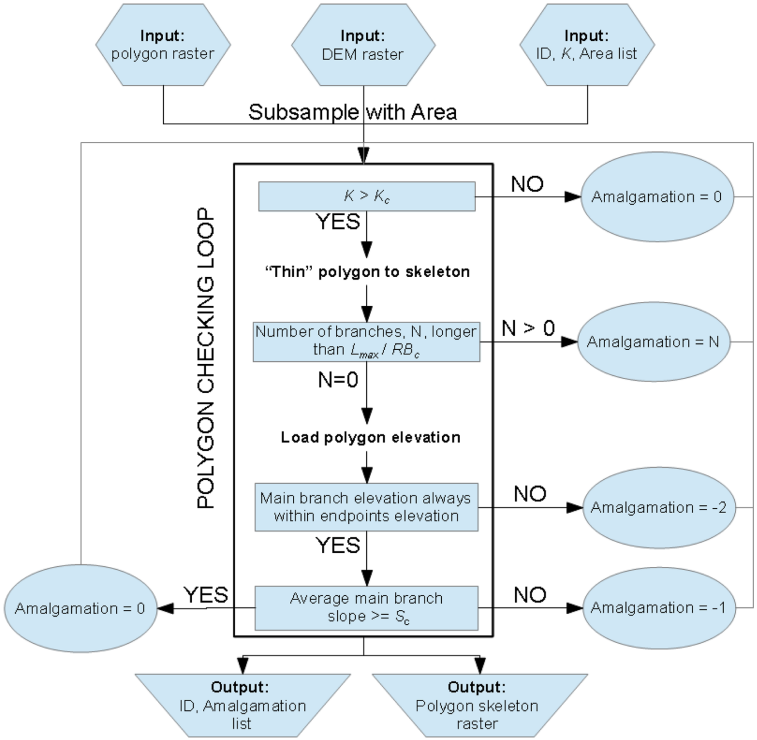


**Figure 4.** Flowchart of the algorithm for automatic detection of amalgamation. Inputs are used to individually analyse polygons based on geometric and topographic characterictics, following a series of conditional tests that lead to a polygon score. A score of zero means that the polygon is considered clean and any other scores refer to some sort of amalgamation. $K$ is the equivalent ellipse aspect ratio (see Eq. 3), $L_{max}$ is the length of the longest branch of a polygon, $RB_c$ is an arbitrary critical length ratio and $S_c$ is a critical slope angle.





NHESSD
2, 7651–7678, 2014



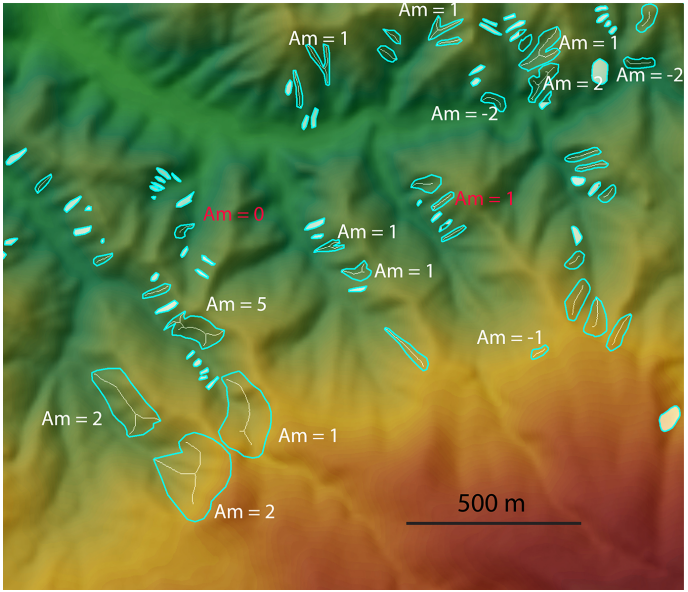


**Figure 5.** Part of the Northridge landslide polygon inventory overlaid on a hillshaded DEM. The skeleton raster output is shown for all polygons larger than 1000 $m^2$ and with $K \geq 2$ (35 polygons). Polygons with $K < 2$ are filled in white and considered clean. White labels show erroneous polygons detected by the algorithm, with positive numbers giving the number of secondary branches detected, −2 meaning ridge or river crossing and −1 indicating a slope smaller than 12°. Red labels show wrongly diagnosed or dubious results within this sample. Polygons with skeleton but no labels have been correctly classified as unamalgamated.





NHESSD
2, 7651–7678, 2014